Biointerface Research in Applied Chemistry
Open-Access Journal (ISSN: 2069-5837)

*Article*
**Volume 13, Issue 4, 2023, 333**
https://doi.org/10.33263/BRIAC134.333

# Synthesis, Characterization, Antioxidant and Antibacterial Activities of Six Metal Complexes Based Tetradentate Salen Type Bis-Schiff Base

**Bouchra Es-Sounni [1,*], Asmae Nakkabi [1], Aziz Bouymajane [2], Ibtissam Elaaraj [1], Mohamed Bakhouch [3], Fouzia Rhazi Filali [2], Mohamed El Yazidi [4], Noureddine El Moualij [1], Mohammed Fahim [1,*]**

[1] Laboratory of Innovative Materials and Biotechnology of Naturel Resources, Faculty of Sciences of Meknes, Moulay Ismail University, Morocco; bouchrasounni@gmail.com (B.E.-S.);
[2] Microbiology and Health Team, Department of Biology, Faculty of Sciences of Meknes, Moulay Ismail University, Morocco; fouzia.filali@yahoo.fr (F.R.F.);
[3] Laboratory of Bioorganic Chemistry, Department of Chemistry, Faculty of Sciences, Chouaïb Doukkali University, P.O. Box 24, El Jadida M-24000, Morocco; bakhouch.m@ucd.ac.ma (M.B.);
[4] University Sidi Mohamed Ben Abdellah, Faculty of Sciences Dhar EL Mahraz, Engineering Laboratory of Organometallic and Molecular Materials and Environment, P.O. Box 1796 (Atlas), 30000 Fez, Morocco; elyazidimohamed@hotmail.com (M.E.Y.);
* Correspondence: mo.fahim@yahoo.fr (M.F.);

Scopus Author ID 24378408300
**Received: 8.05.2022; Accepted: 24.06.2022; Published: 11.09.2022**

**Abstract:** Considering the importance of metal complexes in the development of medicinal chemistry, a series of transition metal complexes of Co(II), Fe(II), Zn(II), Cu(II), and Ni(II) has been synthesized from N,N'-bis(salicylidene)-2,2-dimethyl-1,3-diaminopropane $H_2L$ Schiff base ligand. The reaction of the $H_2L$ with the selected metal ions led to tetrahedral and octahedral coordinated complexes. The structural features of the obtained metal complexes were determined using analytical techniques such as FT-IR, NMR, UV-Vis, X-ray powder diffraction, mass spectrometry, and Thermogravimetry–differential thermal (TGA/DTA) analysis. The measured conductance for obtained compounds has shown the electrolytic behavior of all obtained complexes. The synthesized ligand and corresponding complexes were screened for their antioxidant and antibacterial activities. Indeed, Co(II) and Fe(II) complexes have shown excellent antioxidant activities for DPPH radical scavenging and FRAP assays, respectively. The results obtained from the disc diffusion assay showed that Co(II), Fe(II), Zn(II), and Cu(II) complexes had displayed promising antibacterial activity against *Escherichia coli* and *Staphylococcus aureus*, while no effect has been observed on both strains for ligand $H_2L$ and its corresponding Ni(II) complex.

**Keywords:** Schiff base; metal complex; antioxidant activity; antibacterial activity; TGA/DTA; X-ray powder.



## 1. Introduction

Schiff base derivatives have attracted the attention of many researchers due to their potential metal binding properties and wide range of applications [1–4]. These ligands have played a major role in developing coordination chemistry [5,6], and their synthesis has been widely investigated [7]. Schiff bases containing hydroxyl group (OH) obtained from salicylaldehyde and its derivatives also present a particular chelating exhibit important

photochromic and thermochromic properties. In fact, Schiff bases obtained from salicylaldehyde and its derivatives are largely used to synthesize metal complexes with good stability.

On the other hand, transition metal complexes resulting from the coordination between Schiff bases and metal salts have drawn considerable interest in several domains. They are widely reported to display good photochromic [8], catalytic [9–11], and optoelectronic [12] properties. They display also potent biological actions such as antibacterial [13], antifungal [14], anti-inflammatory [15], antiviral [16], antioxidant [17], antiproliferative [18] and anticancer [19], etc.

View this diversity of applications that exhibit Schiff's bases and their corresponding metal complexes, particularly those obtained from diamines and salicylaldehyde. Importance was hence given to studying these systems in our laboratories [20,21].

In this work, we describe the synthesis and characterization of the Schiff base ligand and their corresponding metal complexes. The prepared compounds are well characterized using FT-IR, NMR, UV-Vis, X-ray powder diffraction, and TGA/DTA techniques. The conductance measurement was also performed for all the obtained compounds. The antioxidant activity using DPPH scavenging and FRAP methods and the antibacterial activity were evaluated for all the obtained products. The complexes are soluble exclusively in polar organic solvents and are stable in the air.

## 2. Materials and Methods

### *2.1. Experimental.*

All chemicals were of analytical grade, supplied from Sigma-Aldrich and other commercial sources, and used as received. FT-IR spectra were recorded using a KBr pellet on an FT-IR-4100 JASCO spectrometer over a range of (400–4000) $cm^{-1}$. $^{1}H$ and $^{13}C$ NMR spectra were carried out on BRUKER AVANCE II 300 Ultra Shield spectrometer using $CDCl_3$ as solvent. ESI-MS spectra were carried out on a Micromass Quattro Premier Tandem MS spectrometer. Electronic absorption spectra were recorded in DMSO at room temperature on UWR Spectrophotometer. Molar conductivity of $10^{-3}$ mol. $L^{-1}$ solution of the complexes in DMSO was measured at room temperature with a Deepvision Model-601 digital direct reading deluxe conductivity meter. X-ray analysis diffraction was performed on Bruker advance D8 eco diffractometer (50KV-20 mA) equipped with CuKα radiation source (λ=1.5418 Å).

### *2.2. Synthesis of the ligand $H_2L$.*

In a two-necked flask equipped with a condenser and dropping funnel, a solution of salicylaldehyde (1.19 g, 2 mmol) in ethanol (10 mL) was introduced and refluxed under magnetic stirring. Then, dropwise, a solution of 2,2-dimethylpropane-1,3-diamine (0.5 g, 1 mmol) in 5 mL of ethanol was added. The refluxing continued until the reaction was completed, as evidenced by TLC. Then, the solvent was distilled off under reduced pressure, and the crude product was crystallized in ethanol. The obtained precipitate was isolated by filtration off under vacuum and dried in the desiccator to obtain pure ligand (yield 94%, m.p.: 57 °C).

$^{1}H$ NMR ($CDCl_3$, 300 MHz) (δ, ppm): 1.10 (s, 6H, $(CH_3)_2$); 3.51 (d, 4H, $(CH_2)_2$, $^{4}J$ = 1.07 Hz); 6.91 (dt, 2H, Ar-H, $^{4}J_m$ = 1.06 Hz, $^{3}J_o$ = 6.47 Hz); 7.00 (d, 2H, Ar-H, $^{3}J$ = 8.08 Hz); 7.28 (dd, 2H, Ar-H, $^{4}J_m$ = 1.64 Hz, $^{3}J_o$ = 7.65 Hz); 7.34 (dt, 2H, Ar-H, $^{4}J_m$ = 1.69 Hz, $^{3}J_o$ = 8.40 Hz); 8.35 (s, 2H, CH=N), 13.60 (s, 2H, Ar–OH). $^{13}C$ NMR ($CDCl_3$, 75 MHz) (δ, ppm): 24.49

($(CH_3)_2$); 36.26 ($C(CH_3)_2$); 68.13 ($(CH_2)_2$); 117.06; 118.59; 118.74 (C-CH=N); 131.38; 132.65; 161.22 (C-OH); 166.05 (CH=N). IR (KBr) ν ($cm^{-1}$): 3423 (OH), 1632 (CH=N), 1278 (C–O). UV–Vis bands ($\lambda_{max}$, nm, (ε, $M^{-1}$ $cm^{-1}$): π→π*, 257 (15300), 301 (6800); n→π*, 360 (3700); CT, 441 (510). Color: Yellow.

*2.3. Synthesis of metal complexes ML.*

In a single-necked flask, an ethanolic solution of ligand $H_2L$ (1 mmol) was added to appropriate metal salt $MCl_2$, $xH_2O$ (1 mmol), and two drops of triethylamine. The mixture was refluxed under magnetic stirring until the consumption of the synthons. After, the solvent was eliminated through a rotary evaporator. The obtained solid was then filtered and washed with diethyl ether and cold ethanol. The solid was recrystallized, if necessary, in ethanol to obtain the desired pure complex ML.

[CuL] complex: FW: 371.92 g/mol. IR (KBr) ν ($cm^{-1}$): 3415 (OH), 1624 (CH=N), 1388 (C–O), 610 (O-Cu), 534 (N-Cu). UV–Vis bands (λmax, nm, (ε, $M^{-1}$ $cm^{-1}$): π→π*, 265 (12800), 280 (12000); n→π*, 313 (6900); CT, 401 (490); d-d, 642 (10). Color: Dark green.

[NiL] complex: FW: 367.07 g/mol. IR (KBr) ν ($cm^{-1}$): 1611 (CH=N), 1445 (C–O), 686 (O-Ni), 626 (N-Ni). UV–Vis bands (λmax, nm, (ε, $M^{-1}$ $cm^{-1}$): π→π*, 280 (6700), 296 (8100); n→π*, 350 (7200); CT, 385 (1000); d-d, 631 (400). Color: Brown.

[$FeLCl_2$] complex: FW: 435.13 g/mol. IR (KBr) ν ($cm^{-1}$): 3449 (O-H), 1615 (CH=N), 1312 (C–O), 534 (O-Fe), 449 (N- Fe). UV–Vis bands (λmax, nm, (ε, $M^{-1}$ $cm^{-1}$): π→π*, 254 (12000), 272 (9400); n→π*, 300 (6000); CT, 369 (3000); d-d, 551 (1000). Color: Garnet.

[ZnL] complex: FW: 446.68 g/mol. IR (KBr) ν ($cm^{-1}$): 3449 (OH), 1617 (CH=N), 1250 (C–O), 678 (O-Zn), 578 (N-Zn). UV–Vis bands (λmax, nm, (ε, $M^{-1}$ $cm^{-1}$): π→π*, 256 (12000), 270 (13000); n→π*, 300 (7100); CT, 377 (1100). Color: Yellowish.

[$CoLCl_2$] complex: FW: 447.24 g/mol. IR (KBr) ν ($cm^{-1}$): 3445 (OH), 1620 (CH=N), 1090 (C–O), 572 (O-Co), 460 (N-Co). UV–Vis bands (λmax, nm, (ε, $M^{-1}$ $cm^{-1}$): π→π*, 234 (3400), 259 (3200); n→π*, 283 (2800); CT, 414 (320); d-d, 671 (110). Color: Green.

*2.4. In vitro antioxidant activity assays.*

The antioxidant capability of the ligand and their metal complexes were investigated by two in vitro methods; the DPPH method is related to radical scavenging characterization of pure compounds, and the FRAP method is related to reduction antioxidant characterization.

2.4.1. DPPH radical scavenging method.

The free radical scavenging was measured by the 2,2-diphenyl-1-picrylhydrazyl ($DPPH^{\bullet}$) using the protocol described by Blois [22]. According to this method, 24 $mg.L^{-1}$ solution of the DPPH• radical in methanol was prepared, and 2.5 mL of this solution was added to the solution (1 mL) of the tested compounds in methanol at different concentrations (100, 300, 500, 700, 900, 1000 μg/mL). The mixture was shaken vigorously and allowed to stand in the dark at room temperature for 30 minutes. Then, the absorbance at 517 nm was measured by a spectrophotometer. Lowering the absorbance of the reaction mixture indicated a higher free radical scavenging activity. MeOH, DPPH solution, and ascorbic acid were used as blank, control, and standard, respectively.

The following equation was used to calculate the percentage of ability to scavenge the DPPH radical (RSA %):

$$DPPH\bullet\ scavenging\ activity\ (\%) = \left(\frac{A_0 - A_1}{A_0}\right) \times 100$$

where $A_0$ is the absorbance of the control solution, and $A_1$ is the absorbance in the presence of sample solutions or standards for positive control.

2.4.2. FRAP method.

The antioxidant potential of the ligand $H_2L$ and their metal complexes ML were determined by a FRAP method; the antioxidant molecules usually transfer a single electron to act as a reducing agent of Fe(III) to Fe(II). The modified method of ferric reducing antioxidant power (FRAP) provided by Benzie and Strain has been used to perform this assay [23]. For this purpose, the ligand, metal complexes, and standard antioxidants were prepared in 1 mL of distilled water in different concentrations (100-1000 µg/mL). 1 mL of potassium ferricyanide (1%) and sodium phosphate (pH = 6.6) were added to the tested samples. After incubation at 50 °C (20 min), 1 mL of TCA solution (10%) was added to stop the reaction to the mixtures. Finally, the reaction was completed by adding 0.25 mL of $FeCl_3$ (0.1%), and the absorbance was measured at 700 nm. Greater reducing power was shown by the higher absorbance of the reaction mixture.

*2.5. In vitro antibacterial assay.*

The antibacterial activity of Schiff's base ligand $H_2L$ and their corresponding metal complexes (ZnL, CuL, $FeLCl_2$, $CoLCl_2$, and NiL) was evaluated against Escherichia coli and Staphylococcus aureus using the disc diffusion method described by the Clinical and Laboratory Standards Institute guidelines [24]. Bacteria were cultured overnight at 37 °C for 24 h on Mueller Hinton agar, then adjusted with sterile water to a concentration of 108 $CFU.mL^{-1}$ using 0.5 McFarland as a standard. 1 mL of this bacterial suspension was used to inoculate Petri dishes containing Mueller Hinton agar. Then, the sterile filter discs (6 mm in diameter) were placed on the surface of the Petri dishes, and 10 µL of Schiff's stock solution at a concentration of 20 mg/mL (chosen as the minimum inhibitory concentration) was added to the filter disc. DMSO and Imipenem served as negative and positive controls, respectively. After incubation of the Petri dishes at 37 °C for 24 hours, the diameters of the zones of inhibition were measured in millimeters. All experiments were done in triplicate.

## 3. Results and Discussion

The reaction between the N,N'-bis(salicylidene)-2,2-dimethyl-1,3-diaminopropane H2L Schiff base ligand was prepared by the reaction 2,2-dimethyl-1,3-diaminopropane and salicylaldehyde in refluxed ethanol. The ligand was then condensed with different metal salts to afford the targeted metal complexes ML according to the synthetic pathway in Scheme 1.

*3.1. Conductance measurements.*

The molar conductance ($\Lambda m$ = k/C) of ligand $H_2L$ and their corresponding complexes ML were measured at room temperature in DMSO solution ($10^{-3}$ mM) (Table 1). The molar conductance values obtained for all compounds are between 18.9 and 35.4 $\Omega^{-1}$ $cm^2$ $mol^{-1}$ which implies their non-electrolytic nature [25].

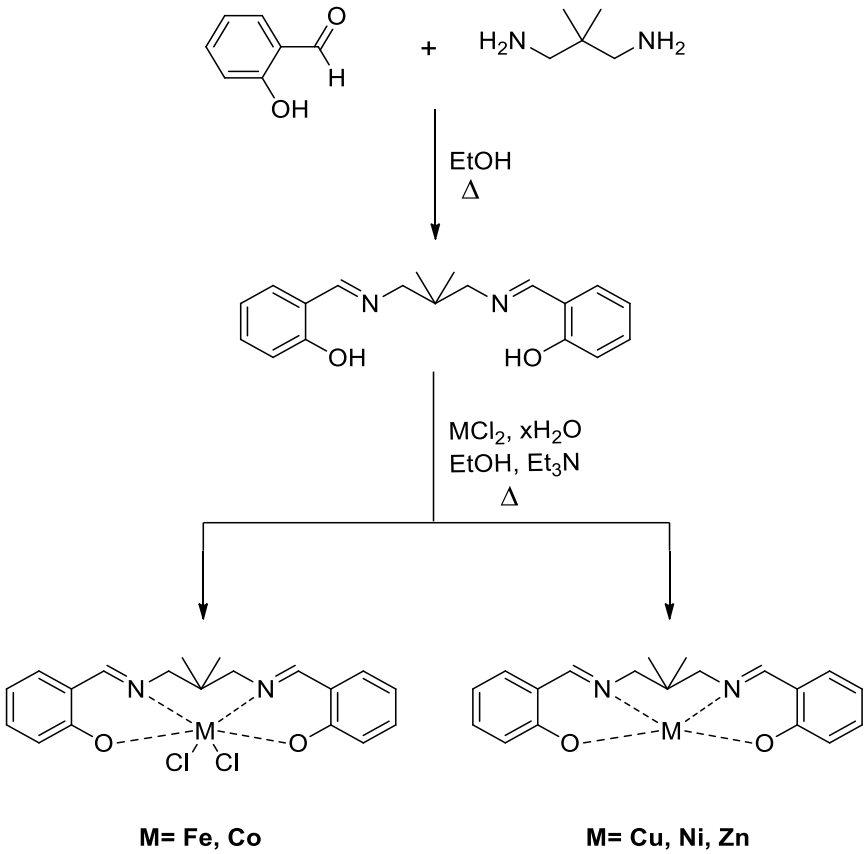


**Scheme 1.** Synthetic pathways of ligand $H_2L$ and metal complexes.

*3.2. TGA/DTA analysis.*

The thermal stability of $H_2L$ and their metal complexes have been investigated based on the TGA and DTA method within a temperature range from room temperature to 1000 °C. The TGA/DTA curves of compounds are presented in Figure 1. The curves indicated the absence of hydrated and coordinated water and revealed that all complexes are stable until 300°C and show a stage of decomposition after this temperature. The decomposition of the residual complexes occurred at higher temperatures (300-772°C).

*3.3. Spectroscopic studies.*

3.3.1. FT-IR spectroscopy.

The synthesized compounds' IR spectra (Figure 2) show the presence of all the desired functional groups. In order to confirm the chelation of the ligand $H_2L$ to metal ion M(II), IR spectra of complexes ML were compared to that of the free ligand $H_2L$. For complexes, IR spectra show a weak band between 1611 and 1624 $cm^{-1}$ assigned to $\nu_{(C=N)}$ vibration, whereas it appears at 1632 $cm^{-1}$ for the free ligand $H_2L$. This negative shift $\Delta\nu_{(C=N)}$ = 8 to 23 $cm^{-1}$ can be attributed to the electron-withdrawing effect of the coordinated metal, which decreases electron density in the imine bond and lead to a lower $\nu_{(C=N)}$ frequency. This suggests the involvement of the nitrogen atom of the imine group in complexation with metal ions. The complexation of the ligand $H_2L$ with metal ions can be further confirmed by the appearance of new bands between 534–686 $cm^{-1}$ and 449–626 $cm^{-1}$ belonging to $\nu_{(M-O)}$ and $\nu_{(M-N)}$ [29], respectively. Hence, IR data shows clearly that the ligand $H_2L$ act as a dianionic tetradentate ligand ($N_2O_2$), having O (phenolate) and N (imine) as coordination sites.

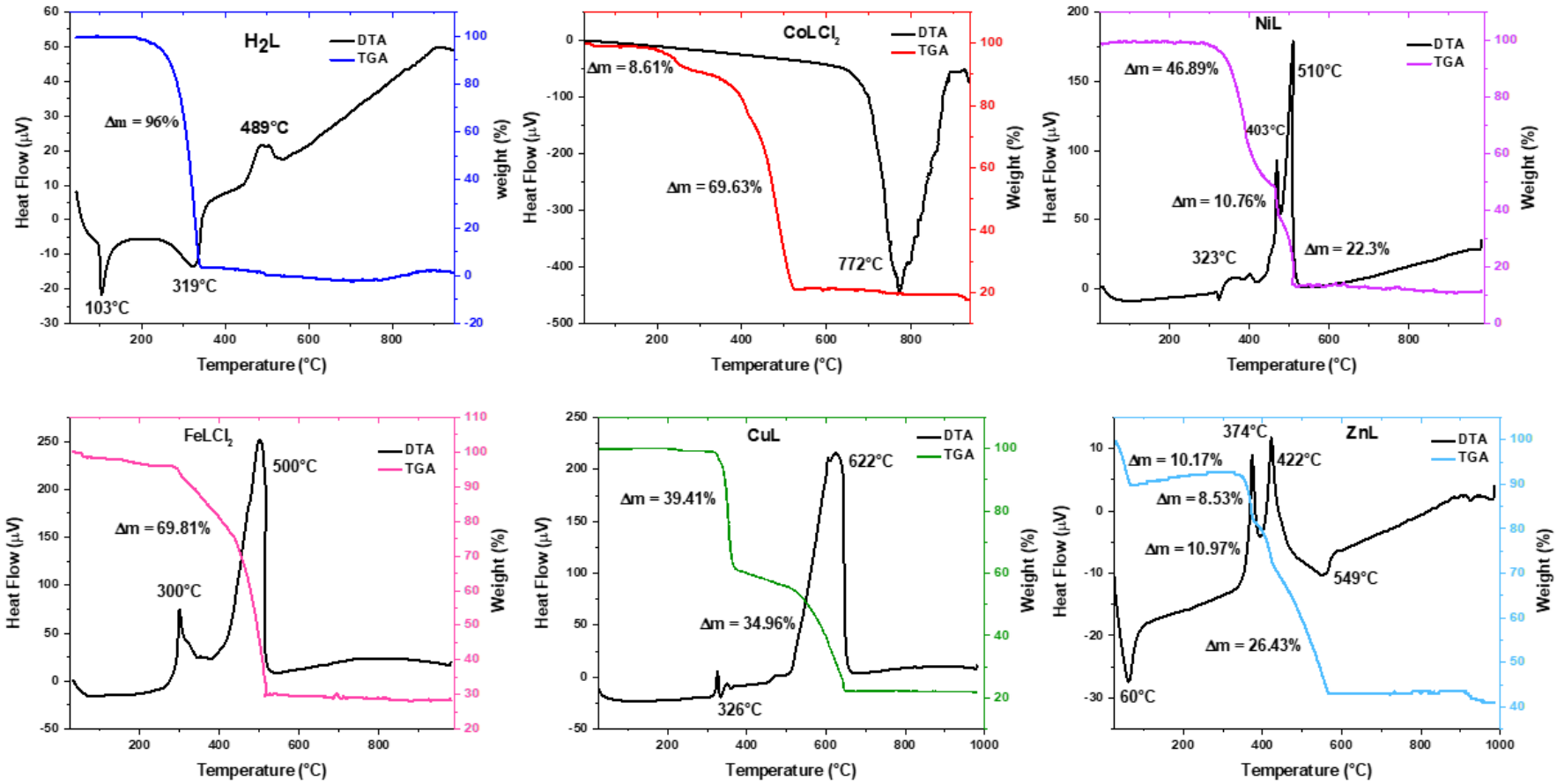


**Figure 1.** DTA/TGA curves of $H_2L$ and their metal complexes ML.

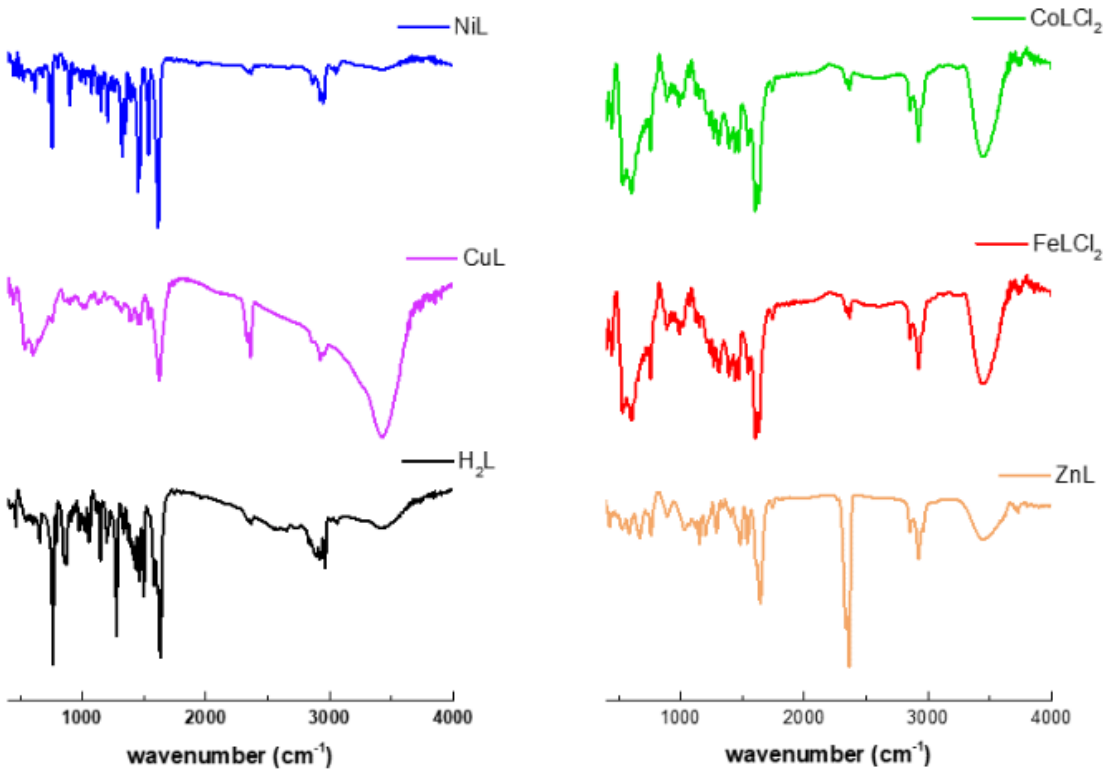


**Figure 2.** IR spectra of ligand $H_2L$ and their metal complexes.

3.3.2. ESI-Mass spectral studies

The mass spectra of ML complexes present molecular ion peaks relative to the structures $[ML]^{+\cdot}$, confirming the molecular weight of the obtained complexes. The spectra also show a peak at *m/z* = 311 Da relative to the mass of the compound $[H_2L]^{+\cdot}$. The mass spectrometry data are in good agreement with the proposed structures. The plausible fragmentations pathway is illustrated in Scheme 2.

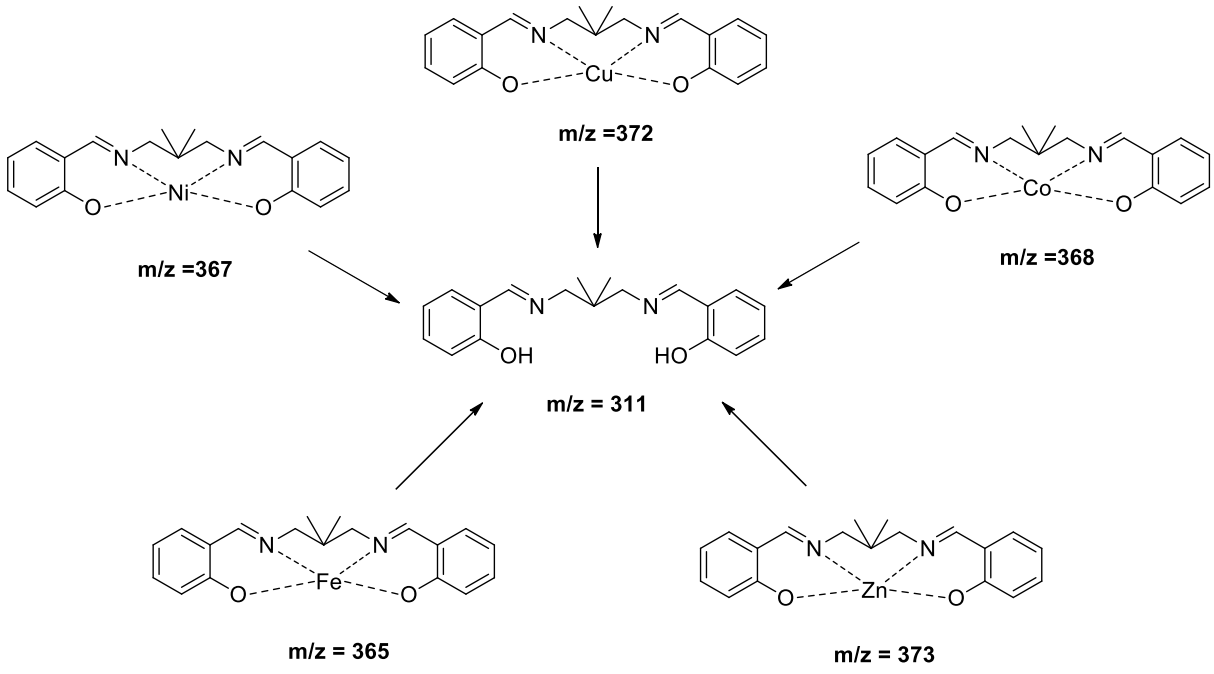


**Scheme 2.** Plausible fragmentation pathways of obtained complexes ML.

3.3.3. UV-Visible spectra.

The UV-Vis spectra of ligand and metal complexes ML were recorded in DMSO (10-4 M) at 298 K in 200 – 800 nm (Figure 3). Relevant electronic spectra data are presented in Table 1.

The ligand showed four absorption bands that appeared in the range of 257 – 414 nm. The first band assigned to π→π* transition related to molecular orbitals localized on phenolic chromophore. The second and the third bands are attributed to π→π* and n→π* transitions of imine chromophore. The lower energy of the observed fourth band may be related to charge transfer transitions from bonding orbital of donor atom of ligand to non- or anti-bonding orbital of metal (LMCT) or metal to ligand (MLCT) [26].

The absorption spectra for the metal complexes ML shows an additional weak band in the range of 500-700 nm, which could be assigned to the d-d transition. Indeed, Cu(II) complex spectrum shows a band at 642 nm due to $^{2}T_{2}(D) \rightarrow {}^{2}E(D)$ transition indicating the tetrahedral geometry of the complex. Ni(II) complex spectrum displays a band at 631 nm, assigned to $^{3}A_{2g}(F) \rightarrow {}^{3}T_{2g}(F)$ transition for the tetrahedral geometry.

Co(II) complex and Fe(II) complex spectra present d-d transition bands d-d at 671 and 551 nm, attributed to $^{4}T_{1g}(F) \rightarrow {}^{4}T_{2g}(F)$ and $^{5}T_{2}(D) \rightarrow {}^{5}E(D)$ transition, respectively.

Moreover, the π→π* and n→π* transitions observed in the spectrum of the ligand were shifted to longer wavelength (bathochromic effect) values along with lower intensities which confirm the chelation of the ligand with metal ions.

**Table 1.** Electronic absorption data of $H_2L$ ligand and ML complexes.

| Compound | Absorption ($\lambda_{max}$, nm) | | | | | Conductance ($\Omega^{-1}$ cm$^2$ mol$^{-1}$) |
|---|---|---|---|---|---|---|
| | π→π* (benzene) | π→π* (CH=N) | n→π* | CT | d→d | |
| $H_2L$ | 257 | 301 | 360 | 441 | - | 33.8 |
| $CoLCl_2$ | 234 | 259 | 283 | 414 | 671 $^{4}T_{1}g(F) \rightarrow {}^{4}T_{2}g(F)$ | 35.4 |
| $FeLCl_2$ | 254 | 272 | 300 | 369 | 551 $^{5}T_{2}(D) \rightarrow {}^{5}E(D)$ | 32.3 |
| ZnL | 256 | 270 | 300 | 377 | - | 18.9 |
| CuL | 265 | 280 | 313 | 401 | 642 $^{2}T_{2}(D) \rightarrow {}^{2}E(D)$ | 29.2 |
| NiL | 280 | 296 | 350 | 385 | 631 $^{3}A_{2}g(F) \rightarrow {}^{3}T_{2}g(F)$ | 32.1 |

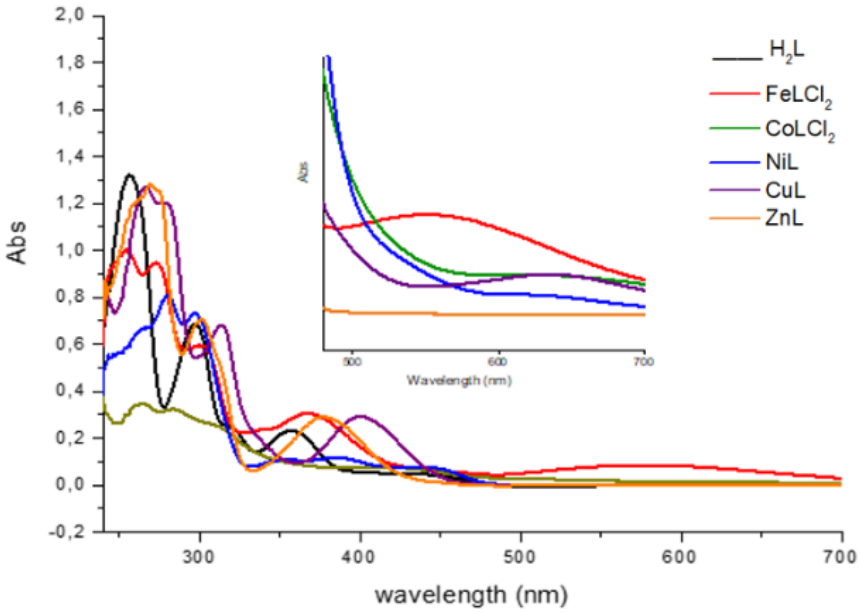


**Figure 3.** UV-Vis spectra of $H_2L$ ligand and their corresponding complexes ML.

3.3.4. X-ray powder.

Shimadzu 6100 diffractometer (Cukα = 1.54060 Å) was used to examine the crystal proprieties of all compounds, X-ray working parameters, which are 40 kV/30 mA, with 0.02° step, with a start of 5° and stop 80° diffraction angle and continuing scanning mode, were used for the measurement taken. The X-ray spectra for the ligand $H_2L$ and their metal complexes ML are presented in figure 4; the crystal data collection and structure solution details are summarized in Table 2.

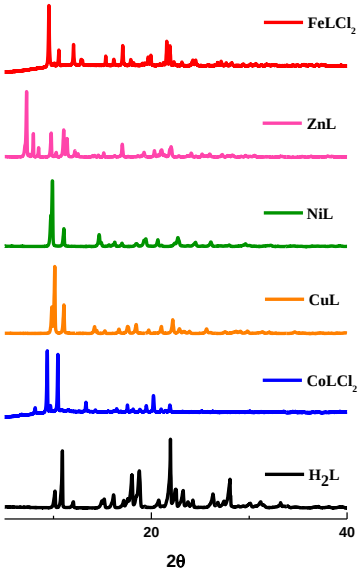


**Figure 4.** X-ray spectrum of $H_2L$ and their metal complexes.

*3.4. In vitro antioxidant activities assays.*

3.4.1. Free radical scavenging activity

The antioxidant activity of Schiff base $H_2L$, Zn(II), Ni(II), Cu(II), Co(II), and Fe(II) metal complexes, together with the standards, were assessed on the basis of the free radical scavenging effect of the stable DPPH free radical activity. The obtained results are gathered in table 3.

The trapping capacity of the tested compounds on the basis of the percentage of inhibition is depicted in figure 5. The outcomes show that the DPPH scavenging activity of metal complexes is much better than the free ligand $H_2L$, whereas it's lower than ascorbic acid (vitamin C) used as a reference. The obtained $IC_{50}$ values for the tested compounds are presented in table 3, along with the correlation coefficient ($R^2$) values. The results show that the $CoLCl_2$ and $FeLCl_2$ complexes exhibit higher antioxidant capability ($IC_{50}$) compared to NiL and ZnL complexes. In addition, all tested complexes exhibit excellent DPPH scavenging power over the free ligand $H_2L$. The order of scavenging potential can be given as follow: vitamin C > $CoLCl_2$ > $FeLCl_2$ > ZnL > NiL > CuL > $H_2L$.

**Table 3.** DPPH scavenging capacities (IC50, $\mu$M) of $H_2L$ ligand and their ML metal complexes.

| | **Compounds** | | | | | | |
|---|---|---|---|---|---|---|---|
| | $H_2L$ | CuL | ZnL | NiL | $CoLCl_2$ | $FeLCl_2$ | Vitamin C* |
| **IC50 ± SD** | - | - | 931 ±0.78 | 996 ±0.84 | 541 ±0.94 | 901 ± 0.62 | 55 ± 0.53 |
| **$R^2$** | 0.987 | 0.948 | 0.974 | 0.991 | 0.988 | 0.998 | 0.960 |

($n$ = 3, $X$ ± SEM); IC50: inhibitory concentration; $R^2$ = correlation coefficient. ∗Standards.

**Table 2.** Crystallographic data for $H_2L$ ligand and their ML metal complexes.

| Cristal Data | $H_2L$ | $FeLCl_2$ | ZnL | NiL | CuL | $CoLCl_2$ |
|---|---|---|---|---|---|---|
| **Chemical formula** | $C_{19}H_{22}N_2O_2$ | $C_{19}H_{20}Cl_2FeN_2O_2$ | $C_{19}H_{20}ZnN_2O_2$ | $C_{19}H_{20}NiN_2O_2$ | $C_{19}H_{20}CuN_2O_2$ | $C_{19}H_{24}Cl_2CoN_2O_2$ |
| **Formula weight (g/mol)** | 310.39 | 435.13 | 446.68 | 367.07 | 371.92 | 474.24 |
| **Cristal system** | Orthorhombic | Monoclinic | Monoclinic | Monoclinic | Monoclinic | Monoclinic |
| **Space groupe** | *P 21 21 21* | *P 21/c* | *P 21/c* | *P 21/c* | *P 21/C* | *C 1 c1* |
| **T(K)** | 296 | 296 | 296 | 296 | 296 | 296 |
| **Wavelenght (A)** | 1.54060 | 1.54060 | 1.54060 | 1.54060 | 1.54060 | 1.54060 |
| **a/Å** | 6.1600 | 12.0280 | 12.3450 | 9.9330 | 9.7450 | 11.6630 |
| **b/Å** | 16.1720 | 17.5330 | 10.3900 | 15.8780 | 17.2280 | 13.2280 |
| **c/Å** | 17.3070 | 16.2590 | 13.5690 | 12.2723 | 11.7297 | 19.6900 |
| **α/ º** | 90.0000 | 90.0000 | 90.0000 | 90.0000 | 90.0000 | 90.0000 |
| **β/ º** | 90.0000 | 106.1800 | 100.1430 | 116.3370 | 116.9130 | 106.2160 |
| **γ/ º** | 90.0000 | 90.0000 | 90.0000 | 90.0000 | 90.0000 | 90.0000 |
| **V (Å$^3$)** | 1724.11 | 3293.00 | 1713.22 | 1734.63 | 1755.98 | 2916.88 |
| **Density (g/cm$^3$)** | 1.20 | 1.62 | 1.60 | 1.41 | 1.41 | 1.70 |

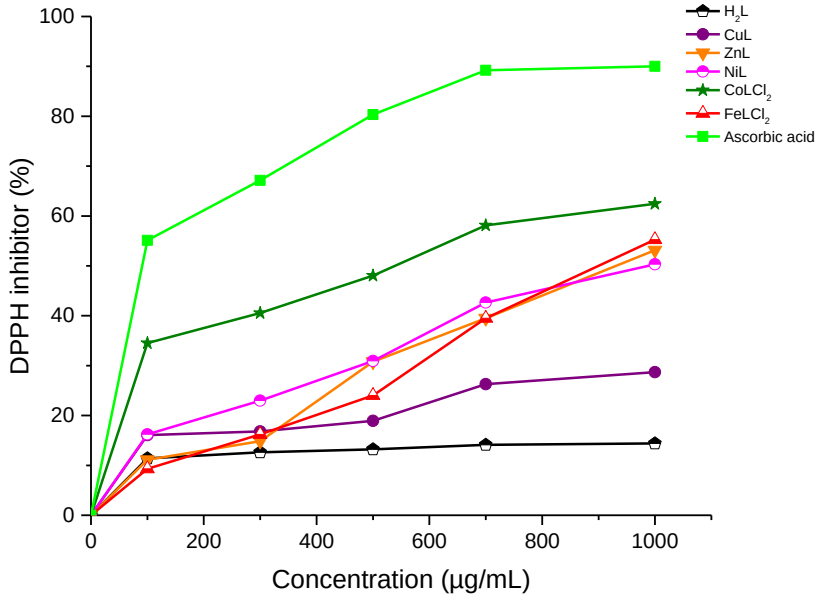


**Figure 5.** DPPH scavenging activity of $H_2L$ Schiff base and their metal complexes.

3.4.2. FRAP method.

The absorbance of the screened compounds was measured at 700 nm (figure 6), indicating that the metal complexes have an excellent reducing potential than $H_2L$ ligand and that they have shown almost half of the standard reduction activities. In addition, $FeLCl_2$ and $CoLCl_2$ show a significant activity compared to other products.

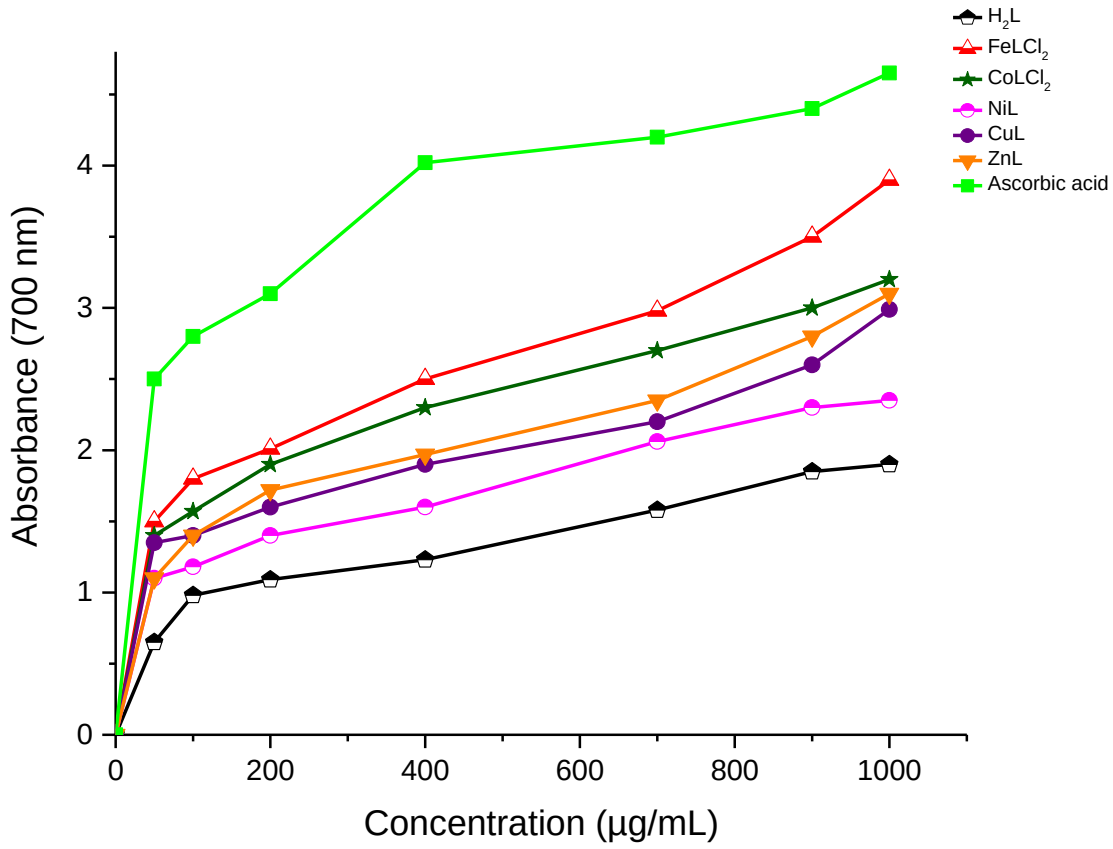


**Figure 6.** Ferric reducing potentials of $H_2L$ ligand and their ML metal complexes.

*3.5. Antibacterial activity.*

The antibacterial activity of Schiff base ligand $H_2L$ and its metal complexes (ZnL, CuL, $FeLCl_2$, $CoLCl_2$, and NiL) at a concentration of 20 mg/mL, against *Escherichia coli* and *Staphylococcus aureus* is illustrated in table 4. It can be shown that the complexes CoL and ZnL with zones of inhibition of 10±0.3 and 12 ± 0.3 mm respectively, were found to be more effective against *Staphylococcus aureus*. The Complexes CuL and $FeLCl_2$ showed less effectiveness against *Escherichia coli* and *Staphylococcus aureus* with the inhibition zones of 8 ± 0.2 and 9 ± 0.1 mm respectively. At the same time, the free ligand $H_2L$ and the NiL complex showed no inhibitory zones against the two tested bacterial strains. Previous studies showed good antibacterial activity of complexes Ni(II), Cu(II), Zn(II), and Fe(II) against *Escherichia coli, Staphylococcus aureus, Pseudomonas aeruginosa, and Bacillus cereus* [27,28]. It is worth noting that metal complexes were more effective against Gram-positive bacteria rather than Gram-negative bacteria. This could be explained by differences in cell wall composition and membrane structure of bacteria; because the Gram-negative bacteria have a thin peptidoglycan layer and an outer lipid membrane, while Gram-positive bacteria have a thick peptidoglycan

layer without an outer lipid membrane [29], as well as the ligand nature, metal nature, chelate effect, the total charge of complexes, and nuclearity of metals in a complex [30,31].

**Table 4.** Antibacterial activity of ligand $H_2L$ and its metal complexes.

| Compounds | Inhibition zone diameter (mm) | |
|---|---|---|
| | ***Escherichia coli*** | ***Staphylococcus aureus*** |
| $H_2L$ | 0 ± 0.0 | 0 ± 0.0 |
| ZnL | 9 ± 0.2 | 12 ± 0.3 |
| CuL | 8 ± 0.2 | 8 ± 0.2 |
| $FeLCl_2$ | 9 ± 0.1 | 9 ± 0.1 |
| $CoLCl_2$ | 7 ± 0.1 | 10 ± 0.3 |
| NiL | 0 ± 0.0 | 0 ± 0.0 |
| Reference drug (Imipenem) | 24 ± 0.1 | 15 ± 0.4 |

## 4. Conclusions

In summary, obtained metal complexes $CoLCl_2$, $FeLCl_2$, ZnL, CuL, and NiL have been synthesized. The structure of the obtained compounds is unambiguously established using analytical methods. The obtained complexes and the free ligand were evaluated for their antioxidant and antibacterial activities. The cobalt complex shows significant antioxidant activity (CMI) among the obtained complexes. Furthermore, except for ligand $H_2L$ and NiL complex, all complexes displayed promising antibacterial activity against *Escherichia coli* and *Staphylococcus aureus*. Regarding the promising result obtained in this work, the described complexes will be the subject of further study to evaluate their biological responses.

## Funding

This research received no external funding.

## Acknowledgments

The authors thank Professor Driss ZAKARIA from Chouaïb Doukkali University for the X-ray measurement.

## Conflicts of Interest

The authors declare no conflict of interest.

## References

1. Ghanghas, P.; Choudhary, A.; Kumar, D.; Poonia, K. Coordination Metal Complexes with Schiff Bases: Useful Pharmacophores with Comprehensive Biological Applications. *Inorganic Chemistry Communications* **2021**, *130*, 108710, https://doi.org/10.1016/j.inoche.2021.108710.
2. Verma, C.; Quraishi, M.A. Recent Progresses in Schiff Bases as Aqueous Phase Corrosion Inhibitors: Design and Applications. *Coordination Chemistry Reviews* **2021**, *446*, 214105, https://doi.org/10.1016/j.ccr.2021.214105.
3. Ceramella, J.; Iacopetta, D.; Catalano, A.; Cirillo, F.; Lappano, R.; Sinicropi, M.S. A Review on the Antimicrobial Activity of Schiff Bases: Data Collection and Recent Studies. *Antibiotics* **2022**, *11*, 191, https://doi.org/10.3390/antibiotics11020191.
4. Alamro, F.S.; Gomha, S.M.; Shaban, M.; Altowyan, A.S.; Abolibda, T.Z.; Ahmed, H.A. Optical Investigations and Photoactive Solar Energy Applications of New Synthesized Schiff Base Liquid Crystal Derivatives. *Sci Rep* **2021**, *11*, 15046, https://doi.org/10.1038/s41598-021-94533-6.
5. Catalano, A.; Sinicropi, M.S.; Iacopetta, D.; Ceramella, J.; Mariconda, A.; Rosano, C.; Scali, E.; Saturnino, C.; Longo, P. A Review on the Advancements in the Field of Metal Complexes with Schiff Bases as Antiproliferative Agents. *Applied Sciences* **2021**, *11*, 6027, https://doi.org/10.3390/app11136027.

6. Singh, A.; Barman, P. Recent Advances in Schiff Base Ruthenium Metal Complexes: Synthesis and Applications. *Top Curr Chem (Z)* **2021**, *379*, 29, https://doi.org/10.1007/s41061-021-00342-w.
7. Iacopetta, D.; Ceramella, J.; Catalano, A.; Saturnino, C.; Bonomo, M.G.; Franchini, C.; Sinicropi, M.S. Schiff Bases: Interesting Scaffolds with Promising Antitumoral Properties. *Applied Sciences* **2021**, *11*, 1877, https://doi.org/10.3390/app11041877.
8. Özdemir, Ö. Bis-Azo-Linkage Schiff Bases—Part(II): Synthesis, Characterization, Photoluminescence and DPPH Radical Scavenging Properties of Their Novel Luminescent Mononuclear Zn(II) Complexes. *Journal of Photochemistry and Photobiology A: Chemistry* **2020**, *392*, 112356, https://doi.org/10.1016/j.jphotochem.2020.112356.
9. De, S.; Jain, A.; Barman, P. Recent Advances in the Catalytic Applications of Chiral Schiff-Base Ligands and Metal Complexes in Asymmetric Organic Transformations. *ChemistrySelect* **2022**, *7*, e202104334, https://doi.org/10.1002/slct.202104334.
10. Yang, X.; Chen, L.; Liu, H.; Kurihara, T.; Horike, S.; Xu, Q. Encapsulating Ultrastable Metal Nanoparticles within Reticular Schiff Base Nanospaces for Enhanced Catalytic Performance. *Cell Reports Physical Science* **2021**, *2*, 100289, https://doi.org/10.1016/j.xcrp.2020.100289.
11. Kaur, M.; Kumar, S.; Younis, S.A.; Yusuf, M.; Lee, J.; Weon, S.; Kim, K.-H.; Malik, A.K. Post-Synthesis Modification of Metal-Organic Frameworks Using Schiff Base Complexes for Various Catalytic Applications. *Chemical Engineering Journal* **2021**, *423*, 130230, https://doi.org/10.1016/j.cej.2021.130230.
12. Amith Nayak, P.H.; Bhojya Naik, H.S.; Teja, H.B.; Kirthan, B.R.; Viswanath, R. Synthesis and Opto-Electronic Properties of Green Light Emitting Metal Schiff Base Complexes. *Molecular Crystals and Liquid Crystals* **2021**, *722*, 67–75, https://doi.org/10.1080/15421406.2020.1868053.
13. Sumrra, S.H.; Zafar, W.; Asghar, M.L.; Mushtaq, F.; Raza, M.A.; Nazar, M.F.; Nadeem, M.A.; Imran, M.; Mumtaz, S. Computational Investigation of Molecular Structures, Spectroscopic Properties, Cholinesterase Inhibition and Antibacterial Activities of Triazole Schiff Bases Endowed Metal Chelates. *Journal of Molecular Structure* **2021**, *1238*, 130382, https://doi.org/10.1016/j.molstruc.2021.130382.
14. Frei, A.; King, A.P.; Lowe, G.J.; Cain, A.K.; Short, F.L.; Dinh, H.; Elliott, A.G.; Zuegg, J.; Wilson, J.J.; Blaskovich, M.A.T. Nontoxic Cobalt(III) Schiff Base Complexes with Broad-Spectrum Antifungal Activity. *Chemistry – A European Journal* **2021**, *27*, 2021–2029, https://doi.org/10.1002/chem.202003545.
15. Ki, J.; Mukherjee, A.; Rangasamy, S.; Purushothaman, B.; Song, J.M. Insulin-Mimetic and Anti-Inflammatory Potential of a Vanadyl-Schiff Base Complex for Its Application against Diabetes. *RSC Adv.* **2016**, *6*, 57530–57539, https://doi.org/10.1039/C6RA11111D.
16. Refat, M.S.; Gaber, A.; Alsanie, W.F.; Kobeasy, M.I.; Zakaria, R.; Alam, K. Utilization and Simulation of Innovative New Binuclear Co(Ii), Ni(Ii), Cu(Ii), and Zn(Ii) Diimine Schiff Base Complexes in Sterilization and Coronavirus Resistance (Covid-19). *Open Chemistry* **2021**, *19*, 772–784, https://doi.org/10.1515/chem-2021-0068.
17. Venkateswarlu, K.; Anantha Lakshmi, P.V.; Shivaraj Synthesis, Spectroscopic and Thermal Studies of Cu+2, Ni+2 and Co+3 Complexes of Schiff Base Containing Furan Moiety. Antitumor, Antioxidant, Antibacterial and DNA Interaction Studies. *Applied Organometallic Chemistry* **2022**, *36*, e6530, https://doi.org/10.1002/aoc.6530.
18. Gowdhami, B.; Manojkumar, Y.; Vimala, R.T.V.; Ramya, V.; Karthiyayini, B.; Kadalmani, B.; Akbarsha, M.A. Cytotoxic Cobalt (III) Schiff Base Complexes: *In Vitro* Anti-Proliferative, Oxidative Stress and Gene Expression Studies in Human Breast and Lung Cancer Cells. *Biometals* **2022**, *35*, 67–85, https://doi.org/10.1007/s10534-021-00351-8.
19. Sun, Y.; Lu, Y.; Bian, M.; Yang, Z.; Ma, X.; Liu, W. Pt(II) and Au(III) Complexes Containing Schiff-Base Ligands: A Promising Source for Antitumor Treatment. *European Journal of Medicinal Chemistry* **2021**, *211*, 113098, https://doi.org/10.1016/j.ejmech.2020.113098.
20. Hajjaji, F.E.; Belghiti, M.E.; Drissi, M.; Fahim, M.; Salim, R.; Hammouti, B.; Taleb, M.; Nahle, A. Electrochemical, Quantum Calculations and Monte Carlo Simulation Studies of N1, N2-Bis (1-Phenylethylidene) Ethane-1, 2-Diamine as a Corrosion Inhibitor for Carbon Steel in a 1.0 M Hydrochloric Acid Solution. *Portugaliae Electrochimica Acta* **2019**, *37*, 23–42, http://dx.doi.org/10.4152/pea.201901023.
21. Mireille Ninon, M.O.; Fahim, M.; Lachkar, M.; Marco Contelles, J.L.; Perles, J.; El Bali, B. Di-hydro-cyclam Dimaleate [H2(Cyclam)(Maleate)2]. *Acta Cryst E* **2013**, *69*, o1574–o1575, https://doi.org/10.1107/S1600536813025580 .
22. Blois, M.S. Antioxidant Determinations by the Use of a Stable Free Radical. *Nature* **1958**, *181*, 1199–1200, https://doi.org/10.1038/1811199a0.

23. Srivastva, A.N.; Singh, N.P.; Shriwastaw, C.K. *In Vitro* Antibacterial and Antifungal Activities of Binuclear Transition Metal Complexes of ONNO Schiff Base and 5-Methyl-2,6-Pyrimidine-Dione and Their Spectroscopic Validation. *Arabian Journal of Chemistry* **2016**, *9*, 48–61, https://doi.org/10.1016/j.arabjc.2014.10.004.
24. Ma, W. Methods for Dilution Antimicrobial Susceptibility Tests for Bacteria That Grow Aerobically : Approved Standard. *CLSI (NCCLS)* **2006**, *26*, M7-A7.
25. Ali, I.; Wani, W.A.; Saleem, K. Empirical Formulae to Molecular Structures of Metal Complexes by Molar Conductance. *Synthesis and Reactivity in Inorganic, Metal-Organic, and Nano-Metal Chemistry* **2013**, *43*, 1162–1170, https://doi.org/10.1080/15533174.2012.756898.
26. Khandar, A.A.; Shaabani, B.; Belaj, F.; Bakhtiari, A. Synthesis, Characterization and Spectroscopic and Electrochemical Studies of New Axially Coordinated Cobalt(III) Salen (Salen=N,N′-Bis(Salicylidene)-1,2-Ethylenediamine) Complexes. The Crystal Structure of [CoIII(Salen)(Aniline)2]ClO4. *Polyhedron* **2006**, *25*, 1893–1900, https://doi.org/10.1016/j.poly.2005.12.001.
27. Naureen, B.; Miana, G.A.; Shahid, K.; Asghar, M.; Tanveer, S.; Sarwar, A. Iron (III) and Zinc (II) Monodentate Schiff Base Metal Complexes: Synthesis, Characterisation and Biological Activities. *Journal of Molecular Structure* **2021**, *1231*, 129946, doi:10.1016/j.molstruc.2021.129946.
28. Shekhar, S.; Khan, A.M.; Sharma, S.; Sharma, B.; Sarkar, A. Schiff Base Metallodrugs in Antimicrobial and Anticancer Chemotherapy Applications: A Comprehensive Review. *emergent mater.* **2021**, https://doi.org/10.1007/s42247-021-00234-1.
29. Kargar, H.; Ardakani, A.A.; Tahir, M.N.; Ashfaq, M.; Munawar, K.S. Synthesis, Spectral Characterization, Crystal Structure and Antibacterial Activity of Nickel(II), Copper(II) and Zinc(II) Complexes Containing ONNO Donor Schiff Base Ligands. *Journal of Molecular Structure* **2021**, *1233*, 130112, https://doi.org/10.1016/j.molstruc.2021.130112.
30. Periferakis, A.; Caruntu, A.; Periferakis, A.-T.; Scheau, A.-E.; Badarau, I.A.; Caruntu, C.; Scheau, C. Availability, Toxicology and Medical Significance of Antimony. *International Journal of Environmental Research and Public Health* **2022**, *19*, 4669, https://doi.org/10.3390/ijerph19084669.
31. Psomas, G.; Kessissoglou, D.P. Quinolones and Non-Steroidal Anti-Inflammatory Drugs Interacting with Copper(II), Nickel(II), Cobalt(II) and Zinc(II): Structural Features, Biological Evaluation and Perspectives. *Dalton Trans.* **2013**, *42*, 6252–6276, https://doi.org/10.1039/C3DT50268F.